On-design and off-design thermodynamic analysis of a hybrid multi-stage solar thermal tower power plant

Rosa P. Merchán[a], María J. Santos[b], Alejandro Medina[c], Irene Heras[d], and Antonio Calvo-Hernández[e]

University of Salamanca, Dpt. of Applied Physics, Salamanca, Spain
[a] *rpmerchan@usal.es (CA),* [b] *smjesus@usal.es,* [c] *amd385@usal.es,* [d] *iheras@usal.es,* [e] *anca@usal.es*

Abstract:

Concentrated solar power (CSP) is one challenging renewable technology for the future production of electricity. Within this concept central receiver solar plants combined with gas turbines are being investigated because of their promising efficiencies and reduced water consumption. Hybrid plants incorporate a combustion chamber in such a way that in periods of low solar irradiance power output can be kept approximately constant and so, electricity production is predictable. An integrated, non-complex solar thermodynamic model of a hybrid multi-stage gas turbine solar plant is developed employing a reduced number of parameters with a clear physical meaning. The solar subsystem is modelled in detail, taking into account the main heliostats field losses factors as cosine effect, blocking, or attenuation. The model is implemented in our own software, developed in Mathematica® language, considering as reference Gemasolar solar field (Seville, Spain). First, an on-design analysis is performed for four different working fluids (dry air, nitrogen, carbon dioxide, and helium), for different number of expansion and compression stages, and for recuperative and non-recuperative modes. Moreover, heliostats field configuration is determined for the design point and its associated efficiency is computed. A pre-optimization process is carried out regarding the pressure ratio of the gas turbine for different configurations. Some significant efficiency and power rises can be obtained when pressure ratio is adapted for each specific configuration and working fluid. Three particular plant configurations are chosen for the off-design analysis due to their interesting behaviours. For these configurations, a dynamic study is performed for four representative of each season. Then, efficiencies and solar share are plotted against time. In addition, fuel consumption and greenhouse emissions are computed for all seasons. Heliostats efficiency varying with the season and the solar time is also forecasted.

Keywords:

Dynamic analysis, On-design pre-optimization, Multi-stage gas turbine, Solar field efficiency, Thermosolar plant.

1. Introduction

The current energetic paradigm of the planet presents lots of challenges worldwide. On one side, the climate change hazard related to pollutant greenhouse emissions produced in combustion of fossil fuels together with the finitude of these fossil resources make necessary a real change in energy paradigm towards cleaner and more reliable energy sources. On the other side, population and energy demand growth emphasize the necessity of new power production means. Concentrated solar power (CSP) plants could fulfil most of these requirements. These systems concentrate unlimited solar energy for heating a fluid, which develops a thermodynamic cycle [1].

Within these systems, plants working under Brayton cycles present all the advantages of gas turbines. Namely, they require less water, which is important for locations with high solar resources and efficiency rates are high due to large working temperatures. Moreover, they stand out due to their flexibility, reliability, and scalability [2].

Another key factor is the hybridization, above mentioned. Hybrid plants allow for a stable power production, removing solar irradiance fluctuations and affording correct night performance [3]. However, these systems are not totally emissions free, but normally natural gas or biogas are employed. Another future option for this issue would consist in employing thermal storage by means of molten salt tanks, as Gemasolar does [4,5].

In these last years, several research projects and some prototypes have been carried out for this kind of plants. Main outcome is that the technology is feasible, but competitive prices must be reached [6]. Therefore, a search for better output records as power output and efficiency results essential. This is the key objective of the present work.

2. Overall plant model

A central solar tower plant hybridized with a combustion chamber and working with a multi-stage gas turbine is considered as the system under study. The combustion chamber allows for a stable production of power output. The system is depicted in Fig. 1, where the three subsystems composing the overall system can be observed: solar part, combustion chamber and heat engine.

Sun radiation is collected by a heliostat field, which concentrates and reflects it into a solar receiver atop the tower. Then, the working fluid takes advantage of the solar heat and it is also heated by the combustion chamber until the desired turbine inlet temperature if necessary. Turbine inlet temperature is considered as a fixed input parameter. So, the working fluid performs a closed irreversible multi-stage Brayton cycle composed of N_c compressors and N_t turbines. Therefore, an intercooler is needed between each pair of compressors for ensuring that the temperature at compressor inlet is always the same. In like manner, a reheater should be placed between each pair of turbines for fixing the same inlet temperature for all turbines.

Main irreversibility sources are included in the thermodynamic model as the non-ideality of compressors, turbines, and heat exchangers, or the pressure decays in both heat absorption and release. Regarding combustion, most important inefficiencies are also made up in the model and natural gas is assumed as fuel. For combustion chamber and for heat engine subsystems, further details of thermodynamic models and analytical calculations can be found in [7]. In Figure 2, a real T-S diagram (and the corresponding reversible one) of the Brayton cycle is shown for a particular case: dry air as working fluid, non-recuperative mode, single-stage configuration and design pressure ratio of 23.4.

The overall thermal efficiency of the system, η, is defined in the usual thermodynamic way as the quotient between the power output, P, and the total energy input of the system (see Eq. (1)). The latter is an addition of both heat sources, solar and combustion. In this way, G accounts for the direct solar irradiance and A_a refers to the aperture area of the solar field.

Regarding the combustion subsystem, the fuel mass flow rate is denoted as $\dot{m}_f$, meanwhile the lower heating value of the fuel is labelled as Q_{LHV}. This overall thermal efficiency can be expressed in an analytical way in terms of the efficiencies of each subsystem, of the heat exchangers that connect

them and of the solar share, f (see Eq. (1)). Heat engine efficiency is denoted as η_h, η_s corresponds to the solar subsystem efficiency, η_c to the combustion chamber efficiency, and ε_{HS} and ε_{HC} are the solar collector and combustion chamber heat exchanger effectiveness, respectively. All these calculations can be found in past works [7-9].

$$\eta = \frac{P}{GA_a + \dot{m}_f Q_{LHV}} = \eta_h \eta_s \eta_c \left(\frac{\varepsilon_{HS} \varepsilon_{HC}}{\eta_c f \varepsilon_{HC} + \eta_s (1-f) \varepsilon_{HS}} \right) \tag{1}$$
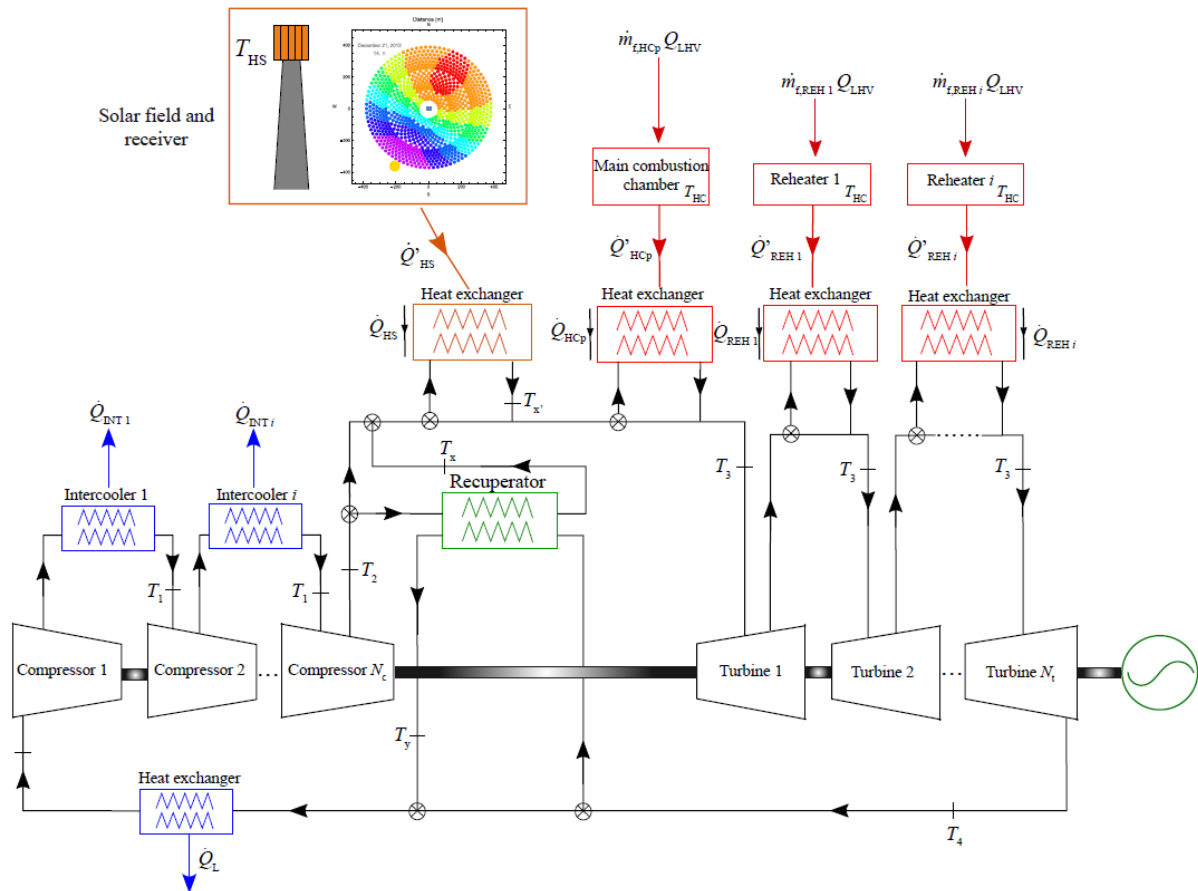

Figure 1. Scheme of the considered thermosolar plant, constituted by three different subsystems: solar subsystem, combustion chamber and heat engine. Main losses and irreversibilities are considered in the model.
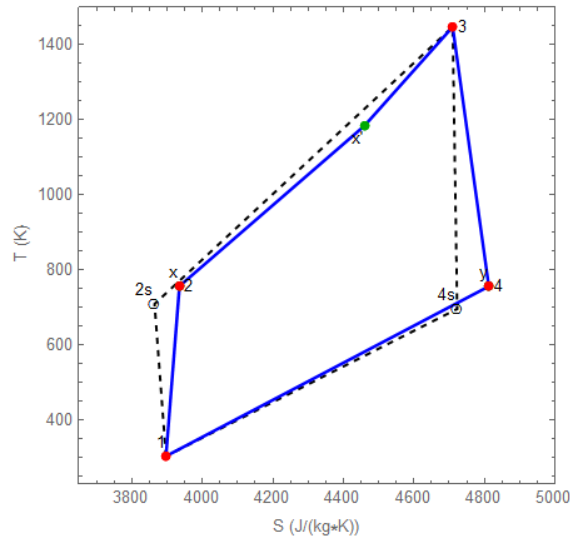
Figure 2. Real T-S diagram (solid line) for dry air as working fluid performing a non-recuperative single stage Brayton cycle ($r_{p,DP}$=23.4). The corresponding ideal cycle is also plotted (dashed line).

In this study, the optical efficiency of the heliostat field, η_0, is computed in detail. Hence, solar field is divided into different rows and, in each row, heliostats are placed considering the space they can occupy during the solar tracking together with a safety distance [10]. Each heliostat has a different efficiency, which also varies with the solar hour and the season of the year, because of their particular location. This efficiency is considered as a product of different losses factors, as it is shown in Eq. (2) and in Fig. 3. The primary contribution to this optical efficiency is the cosine effect ($\cos \omega$) [11], which accounts for the cosine of the incident angle of the Sun radiation in the heliostat surface. It is computed by means of a study of the Sun-heliostat-receiver geometry [12]. Blocking effect measures the amount of lost energy when some part of the radiation coming from a back heliostat reflects in an ahead one. In a similar way, shadowing effect comprehends lost energy due to the shadow projected by a heliostat on another one. Both effects are included in the blocking and shadowing factor, $f_{b,sh}$, which is assumed as a constant factor [10,12,13]. Heliostats present an actual mirror reflectivity, ρ, that defines the amount of solar radiation that they can reflect towards the receiver [10]. When this solar radiations travels towards the receiver, some part of it is absorbed by the ambient air molecules; in such a way that attenuation factor, f_{at}, results in another energy loss [10]. And, the last important energy loss source is the spillage factor, f_{sp}, related to the energy lost due to solar radiation not reaching the absorption area of the receiver, but closer zones [10]. Thus, the optical efficiency of the whole field, η_0, is defined as the average efficiency of each heliostat.

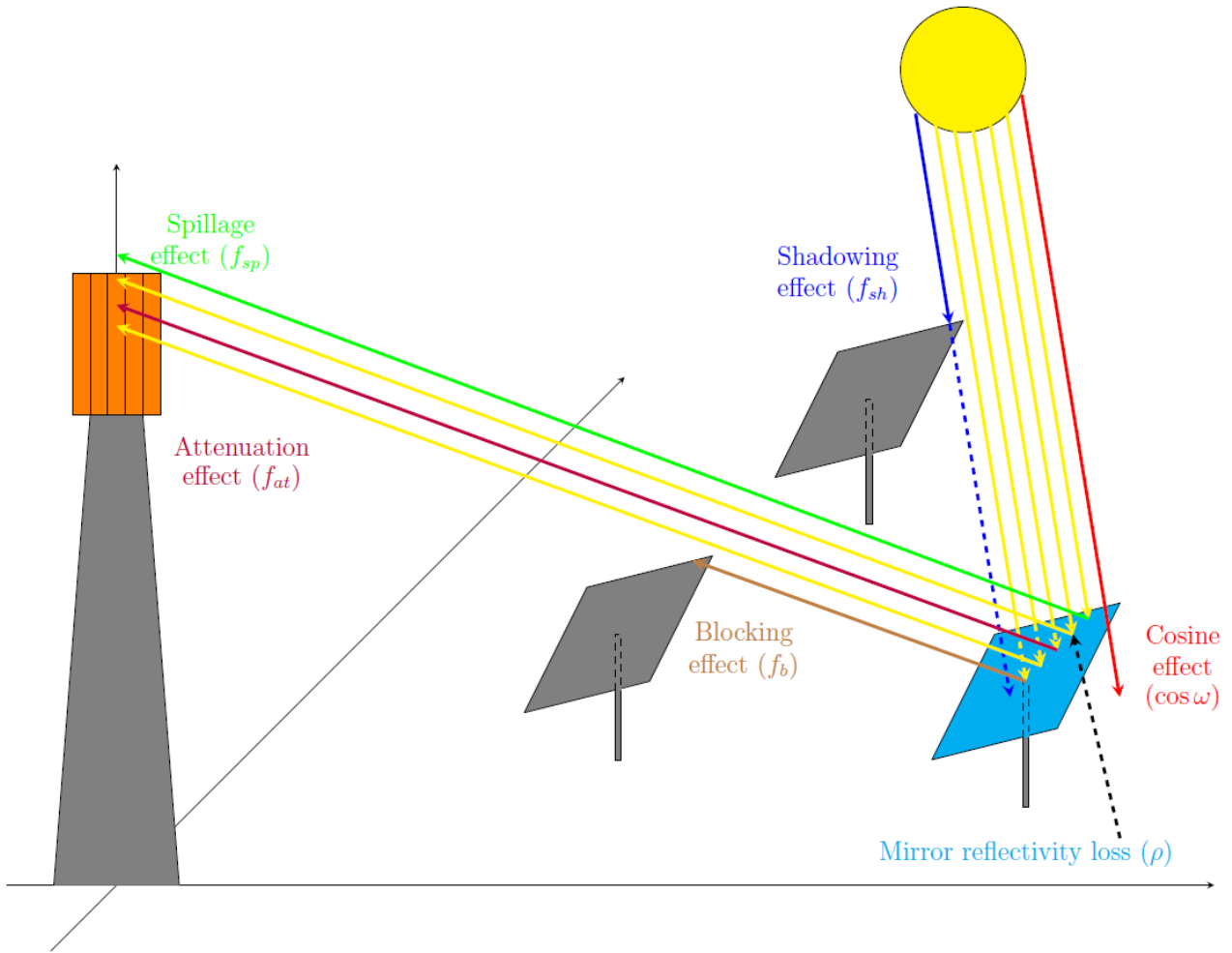$$\eta_{hel} = \cos \omega \times f_{b,sh} \times f_{sp} \times f_{at} \times \rho \qquad (2)$$

Figure 3. Losses factors in the energy transmission process for the system.

3. Numerical considerations

The thermodynamic and optical models have been implemented in Mathematica® software. Brayton cycle model was validated first [7,9] aiming the 5 MW Solugas plant [14,15]. A scaled-up version of Solugas plant is developed here for achieving a commercial scale of power output similar to Gemasolar one (20 MW) [4,5]. Then, most plant dimensions are considered similar to Gemasolar plant. Main difference between this work and Gemasolar plant is precisely the cycle employed in each case: Rankine in Gemasolar and Brayton here. As a consequence, only 1037 heliostats are required here, as it has been proven by means of Thermoflex® software [16], while Gemasolar counts on 2650. It is also important to note that this system works in a hybridized way, meanwhile Gemasolar uses a molten salt storage for non-solar irradiance periods and for stabilizing output power. Meteorological data have been taken from Meteosevilla® database for Gemasolar location (Seville, Spain) [17]. Design point corresponds to June 20th, 2013 at 12:00h, when solar irradiance and ambient temperature are, respectively, G=760 W/m² and T_L=296.5 K.

A circular heliostat field with a central tubular and cylindrical receiver is assumed and solar field data are collected in Table 1. *Solar Titan 250-30000S* gas turbine from Caterpillar® [18] has been chosen with the help of Thermoflex® database due to its particular features. Gas turbine validation predicts a deviation of our Mathematica® simulation of about 0.9% in power output, of 2.4% in thermal efficiency, and of almost 3% in turbine outlet temperature. For other records, lower deviations are found. Therefore, it can be concluded that gas turbine model agrees very well with Thermoflex® data for the dry air mono-stage configuration. Four different working fluids are tested here, three of them work as subcritical fluids: dry air, nitrogen and carbon dioxide; meanwhile, the

other one works as a transcritical one: helium. Further working fluids details are gathered in [7]. The same working fluid mass flow is considered for all cases.

Table 1. *Parameters values for Mathematica® simulation (Gemasolar plant [4,5]).*

Parameter	Value	Unit
Height of the tower	130	m
Height of the receiver	10.5	m
Diameter of the receiver	8.4	m
Height of each heliostat	10.95	m
Width-height ratio of each heliostat	1.0	-
Separation distance between adjacent heliostats	3.285	m
Minimum radius of the heliostat field	65	m
Focusing	Simple	-
Standard deviation due to Sun shape	2.51	mrad
Blocking and shadowing factor	0.95	**-**
Actual mirror reflectivity	0.836	**-**

4. Results

Main plant output records, for both on-design and off-design conditions are discussed next.

4.1. On design analysis and pre-optimization

Design point fixes heliostat field configuration. Figure 4 shows the efficiency of each heliostat at the design point by a colour map. It can be observed that heliostats opposite to the Sun presents higher efficiencies, as it was stated by Stine and Geyer [19]. Average heliostats efficiency is 0.496.

Output records for the four selected working fluids are shown in Figs. 5 and 6 as functions of pressure ratio, r_p. Numbers of turbines and compressors are identical and equal to one, two, three, and infinite. This last case is just a guide to survey the theoretical limits that output records could achieve. Recuperative configurations are considered, although for the single stage case, non-recuperation is also represented. Only in the single stage case, overall thermal efficiency (see Fig. 5) has a maximum in terms of the pressure ratio for He, air, and N_2. For all the other cases, it increases monotonically. The highest efficiency values are found for helium. When a single configuration is assumed, low pressure ratios give better efficiencies in recuperative mode. While, for high pressure ratios, the absence of recuperation leads to higher values of overall performance. Except for carbon dioxide, which is always related to larger efficiencies in recuperative mode. All this performance resembles efficiency curves of Solugas-like system [7].
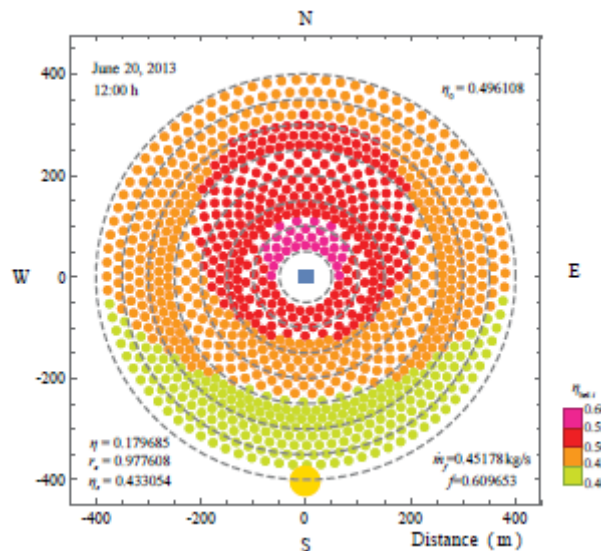
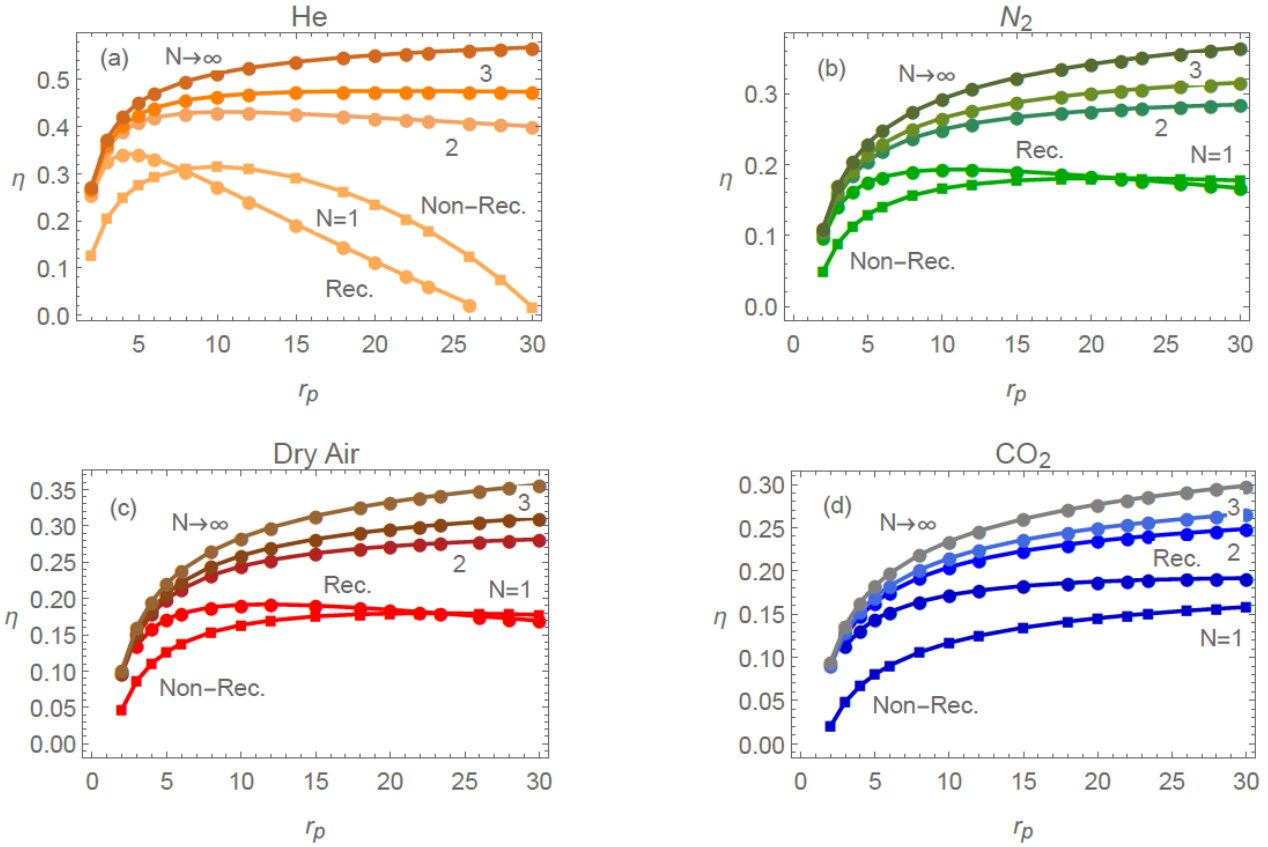Figure 4. Heliostats efficiencies at design conditions.

Figure 5. Overall thermal efficiency, η, versus pressure ratio, r_p, for (a) He, (b) N_2, (c) dry air, and (d) CO_2. One, two, three, and infinite compression and expansion stages are shown ($N=N_c=N_t$). In addition, for N=1, recuperative configurations are marked by circles and non-recuperative ones, by squares.

Solar collector temperature, T_{HS}, is also analysed with the help of Fig. 6. Solar receiver materials impose a temperature limit that could not be surpassed. Therefore, for the sake of materials support, solar collector temperature should be not very large and its control results essential. It can be highlighted that the presence of a recuperator totally changes solar collector temperature behaviour. Monotonic decreasing curves are found for recuperative cases. Meanwhile, the evolution for non-recuperative cases shows an increase of the temperature with the pressure ratio. It is noticeable that, for low pressure ratios, smaller temperatures are associated with single non-recuperative configurations for all working fluids. However, when the pressure ratio increases, recuperative modes lead to smaller temperatures, except for CO_2. On the other side, He is related with the smallest solar collector temperatures, which are below 1000 K for non-recuperative, single-stage and low pressure ratios case. So, as a consequence, in this case, a circular field with a tubular receiver could be feasible. Nonetheless, when other configurations lead to much higher solar collector temperatures, the tubular receiver must be replaced by a cavity one, and, in turn, the circular field by a wedge one.
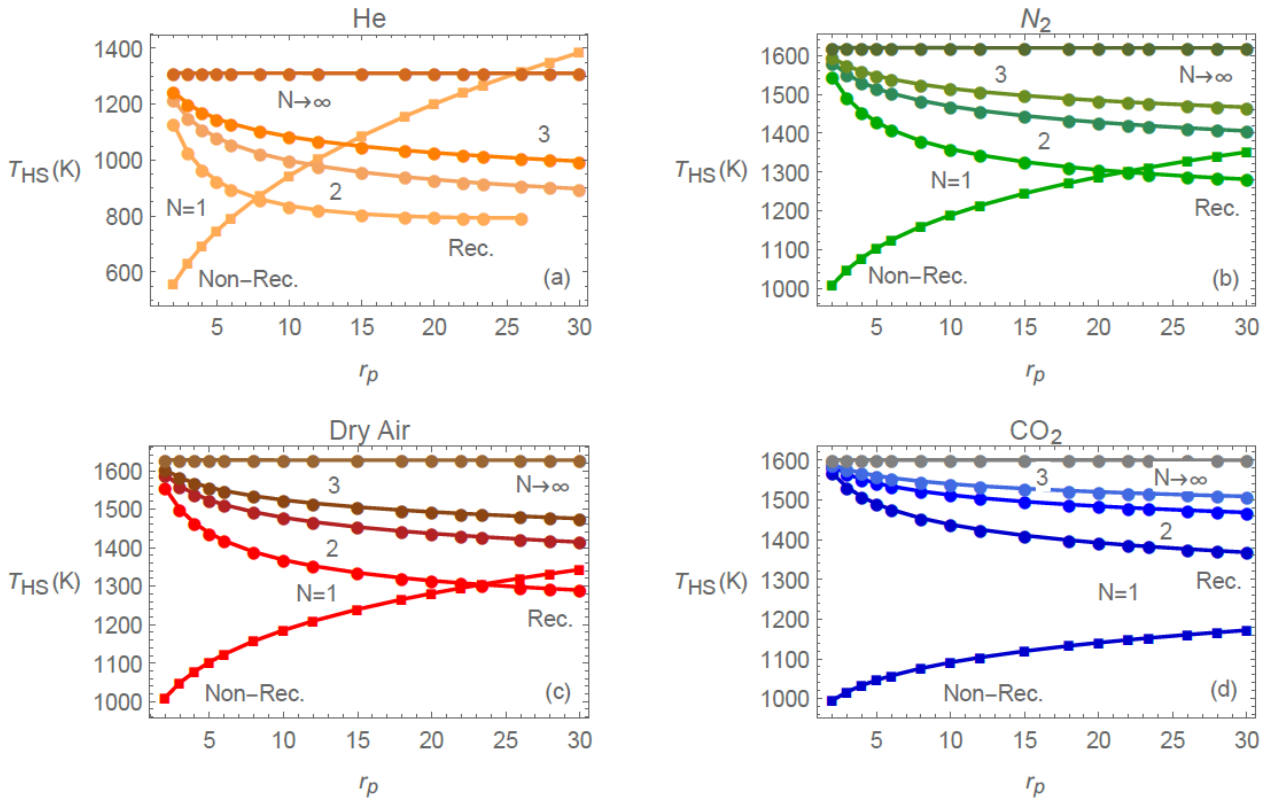
Figure 6. Solar collector temperature, T_{HS}, versus pressure ratio, r_p, for (a) He, (b) N_2, (c) dry air, and (d) CO_2. One, two, three and infinite compression and expansion stages are shown ($N=N_c=N_t$). Recuperative configurations are marked by circles and non-recuperative ones, by squares.

Maximum overall thermal efficiency and its corresponding pressure ratio are shown in Table 2 for three selected configurations, although they have been calculated for the aforementioned four working fluids and for different number of turbines and compressors. These three configurations are: dry air single non-recuperative, dry air two-compression and expansion stages recuperative, and helium single non-recuperative configurations. They have been selected as possible optimum configurations due to a combination of maximum overall thermal efficiency and low solar collector temperature. Moreover, the relative growth of the overall thermal efficiency, of the fuel conversion rate [9] and of the power output are performed with respect to the design pressure ratio of the gas turbine ($r_{p,DP}=23.4$). For instance, adjusting the pressure ratio increases the overall thermal efficiency in only 0.006% for the dry air single non-recuperative case, which means that the pressure ratio was already chosen for obtaining maximum overall efficiency. However, when a second turbine and a second compressor are added and recuperation is taken into consideration, an improvement of almost 57% is achieved. In this case, power output increase is about 91%. For helium working in a single stage and non-recuperative cycle, overall efficiency and power output are enhanced around 76% and 194%, respectively.

Table 2. Relative variations of output records obtained when optimum pressure ratio (with respect to overall thermal efficiency) are selected. Number of turbines and compressors are identical ($N=N_c=N_t$). Rec stands for the presence of recuperator (YR) or for its absence (NR), r_e refers to fuel conversion rate [9] and P is related to power output.

N	Rec	η_{max}	$r_{p,\eta max}$	$\Delta\eta(\%)$	$\Delta r_e(\%)$	$\Delta P(\%)$
				Dry air		
1	NR	0.180	22	0.006	-2.86	0.678
2	YR	0.281	30	56.8	-12.3	91.0
				He		
1	NR	0.315	10	75.8	15.6	194.

4.2. Off-design records

Off-design analysis is performed for four different days corresponding to the start of each season. Solar heliostats field layout was fixed at on-design conditions and Mathematica® simulation allows for calculating heliostats efficiency at whichever hour and season. Then, the seasonal variation of heliostats efficiency can be shown in Fig. 7 at 16:00h. Average efficiency is larger for summer and lower for winter, having intermediate values for autumn and spring, as it was expected.
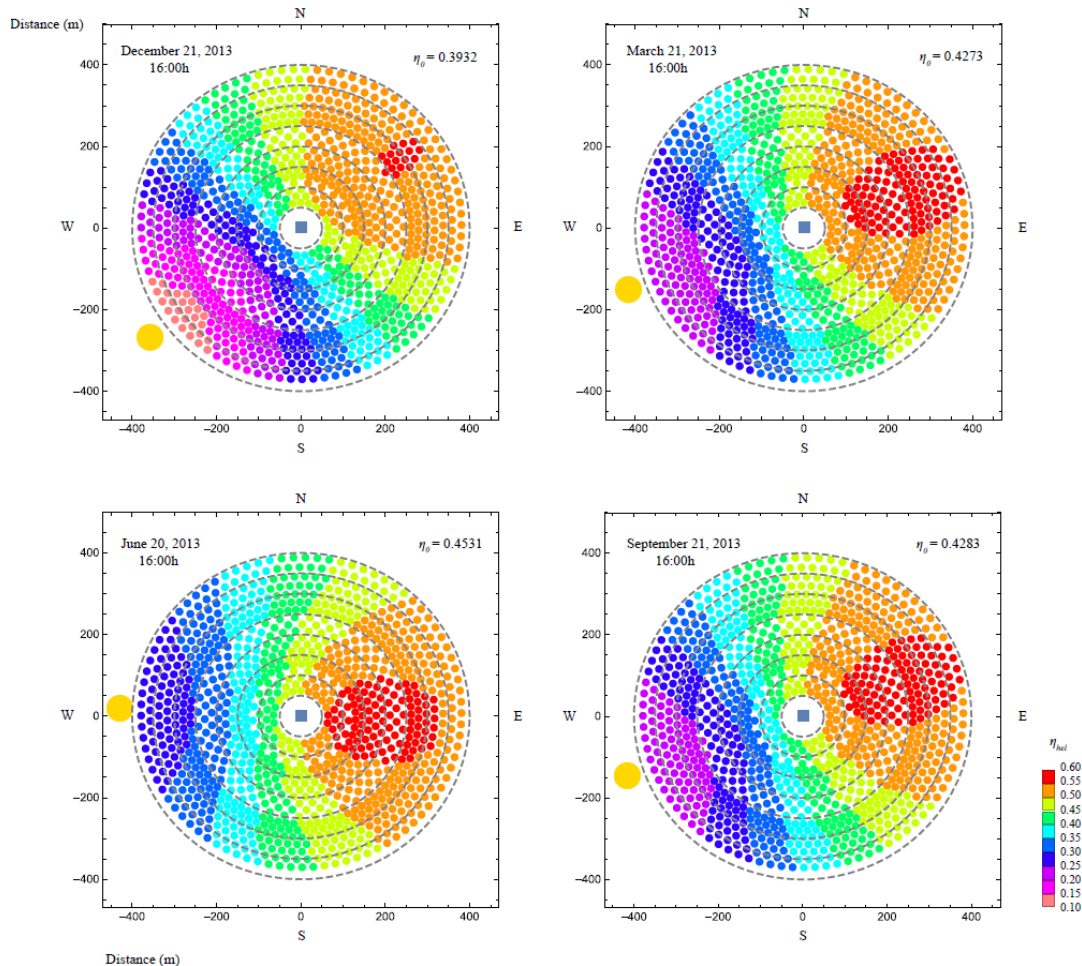

Figure 7. Heliostats efficiencies for (a) winter, (b) spring, (c) summer, and (d) autumn at 16:00h.

In addition, as a consequence of the flexibility of the model, it is possible to compute the daily evolution of all output records for whichever configuration. As an example, the evolution of the main efficiencies throughout a day for the four seasons is shown in Fig. 8 for dry air, single and non-recuperative configuration. The number of functional solar hours is higher in summer than in the other seasons. Fuel conversion rate, r_e, resembles solar direct irradiance curves (meteorological

data can be found in [8]). It can be observed that heliostats optical efficiency, η_0, modulates solar collector efficiency curve, η_s. Furthermore, it was proven that solar share, f, never reaches 1 for the three optimum configurations, so the plant is always working on hybrid mode. More concretely, for He solar share is always below 20%. And He configurations also present the largest values of overall efficiency (η) since solar subsystem contribution and, so, losses are smaller.
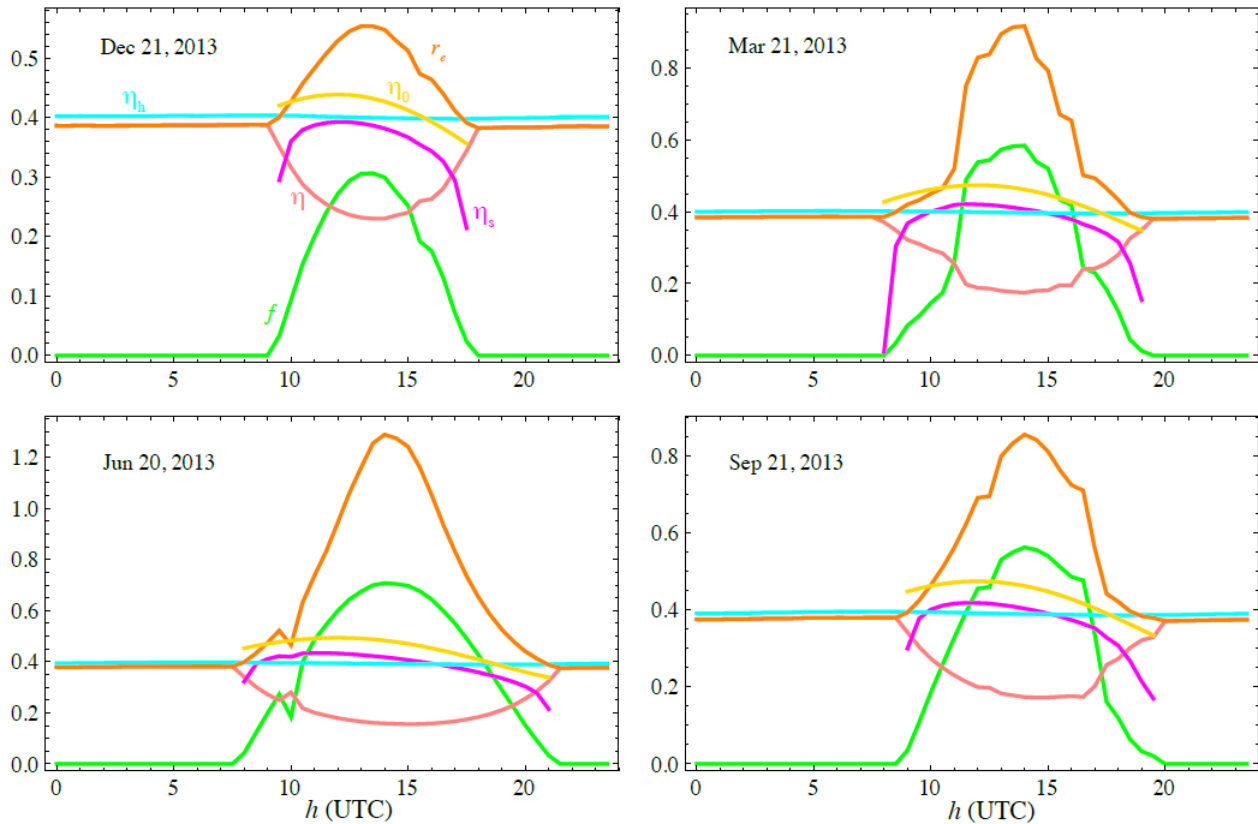

Figure 8. Overall thermal efficiency, η; heat engine efficiency, η_h; solar subsystem efficiency, η_s; heliostat field optical efficiency, η_0; fuel conversion rate, r_e; and solar share, f, versus time in UTC hours for dry air single non-recuperative configuration for: (a) winter, (b) spring, (c) summer, and (d) autumn.

Finally, fuel consumption and carbon dioxide emissions can be calculated during a day for the four seasons (see Fig. 9). Globally, more reduced emissions and obtained for dry air and N=2. Difference between hybrid and non-hybrid modes is larger in summer due to the higher solar irradiance and the higher number of solar hours. This difference is also larger for single non-recuperative configuration with dry air. On the other side, differences between hybrid and non-hybrid natural gas consumption are smaller when dry is substituted by He in accordance with the smaller solar contribution. The same applies to carbon dioxide emissions because they have been calculated taken into account direct conversion factors [8].

Note that all off-design calculations have been performed considering the aforementioned optimum pressure ratios. Although it is not shown here, the consistency of the decision about these optimum pressure ratios throughout any day and whatever season has been proven. In other words, the election of the pressure ratio at design conditions is an acceptable option.
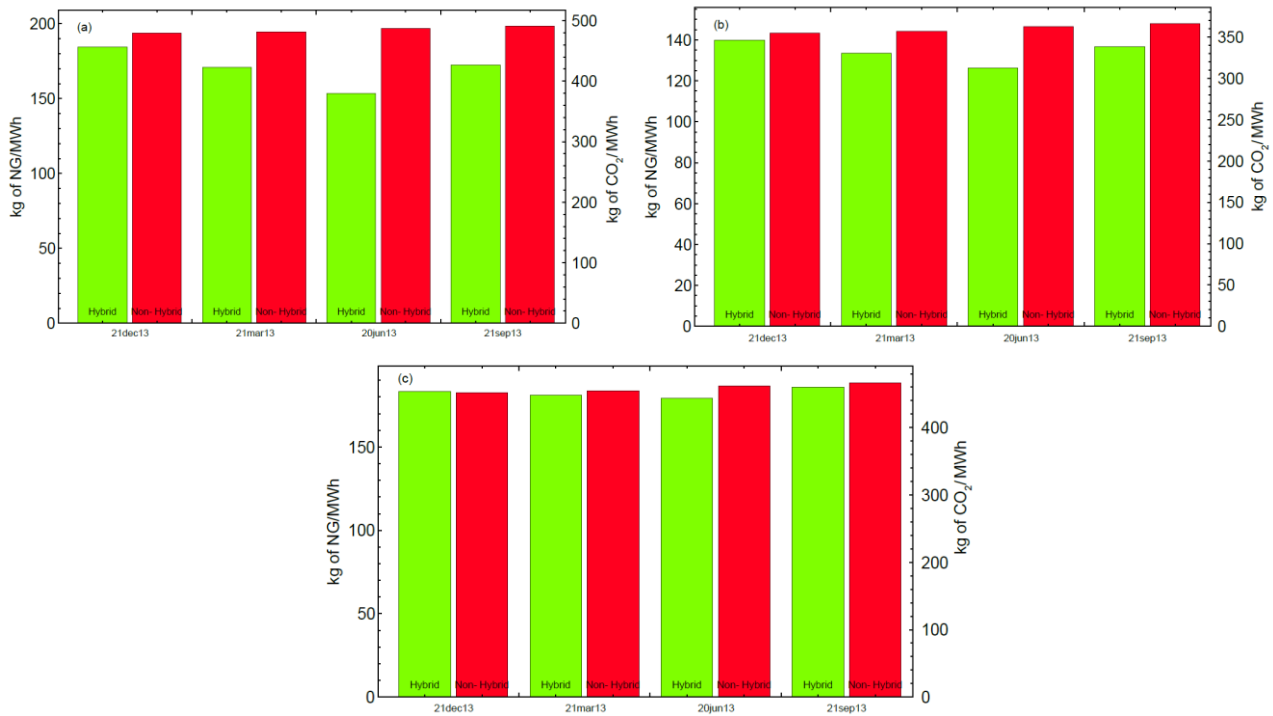
Figure 9. Specific natural gas (NG) consumption and specific CO_2 emissions for (a) dry air, non-recuperative, single stage; (b) dry air, recuperative, N=2; and (c) He, non-recuperative, N=1.

5. Conclusions

A previously developed thermodynamic model for a solar tower hybrid multi-stage gas turbine has been completed with a more comprehensive, but at the same time, simple solar field model. This model takes into account losses factors as spillage, blocking of heliostats, or atmospheric attenuation. After that, a new validation of the model was required. And it was completed by means of Thermoflex® software. A scaled-up evolution of Solugas plant has been performed through a new design based on Gemasolar dimensions. Real solar plant data have been taken from Gemasolar installation.

An analysis of plant output variables at design point has been carried out for different working fluids, for various numbers of compressions and expansion stages, and for recuperation or non-recuperation. It has been proven that helium is associated with higher overall thermal efficiencies than the other fluids, but also with lower solar share. In general, when a single stage configuration is replaced by a two stages one, a considerable increase in the overall thermal efficiency is observed. The presence or absence of a recuperator could also change output records behaviour in a significant amount. In recuperative modes and for low pressure ratios, both overall efficiency and solar collector temperature raise with pressure ratio.

After the on-design analysis, plant performance for any season and any hour can be evaluated. A natural gas consumption and a carbon dioxide emissions reduction of around 20% in summer and of about 10% in winter is achieved for dry air, single stage and non-recuperative configuration.

The analysis performed in this study reflects the necessity of at least three key actions in order to improve the performance of this technology for commercialization in the next future: to increase the materials temperature limits, to enhance solar field design and efficiency for allowing better overall efficiencies, and to look for new power cycle configurations and working fluids.

Acknowledgments

Nomenclature

A_a aperture area of the solar field, m^2

f   solar share

f_{at} attenuation factor

$f_{b,sh}$ blocking and shadowing factor

f_{sp} spillage factor

G   solar direct irradiance, W/m^2

$\dot{m}_f$ total fuel mass flow rate, kg/s

N   number of compression and expansion stages when they are equal

N_c number of compression stages

N_t number of expansion stages

P   power output, W

Q_{LHV} fuel lower heating value, J/kg

r_e fuel conversion rate

r_p pressure ratio

T   temperature, K

t   time, h (UTC)

S   entropy, J/(kg K)

Greek symbols

Δ increment

ε_{HS} solar collector heat exchanger effectiveness

ε_{HC} combustion chamber heat exchanger effectiveness

η overall thermal efficiency

η_c combustion chamber efficiency

η_h heat engine efficiency

η_s solar subsystem efficiency

η_0 optical efficiency of the heliostat field

ρ actual mirror reflectivity

ω Sun radiation incident angle in the heliostat surface, rad

Subscripts and superscripts

DP   design point

L   ambient

max   maximum

References

[1] Weinstein L. A., Loomis J., Bhatia B., Bierman D. M., Wang E. N., Chen G., Concentrating solar power. Chem. Rev. 2015;115:12797-12838.

[2] Olumayegun O., Wang M., Kelsall G., Closed-cycle gas turbine for power generation: a state-of-the-art review. Fuel. 2016;180:694-717.

[3] Okoroigwe E., Madhlopa A., An integrated combined cycle system driven by a solar tower: A review. Renew. Sust. Energ. Rev. 2016;57:337-350.

[4] Burgaleta S., Ramírez D. J. I., Gemasolar, the first tower thermosolar commercial plant with molten salt storage. Proceedings of SolarPACES, Granada, Spain, 2011.

[5]   Relloso E., García E., Tower technology cost reduction approach after Gemasolar experience. Sol. Proc. 2015;69:1660-1666.

[6]   Liu Q., Bai Z., Wang X., Lei J., Jin H., Investigation of thermodynamic performances for two solar-biomass hybrid combined cycle power generation systems. Ener. Conv. Manage. 2016;122:252-262.

[7]   Santos M. J., Miguel-Barbero C., Merchán R. P., Medina A., Calvo Hernández A., Roads to improve the performance of hybrid thermosolar gas turbine power plants: Working fluids and multi-stage configurations. Ener. Conv. Manage. 2018;165:578-592.

[8]   Merchán R. P., Santos M. J., Medina A., Calvo Hernández A., Thermodynamic model of a hybrid Brayton thermosolar plant. Renew. Ener. 2018;128:473-483.

[9]   Olivenza-León D., Medina A., Calvo Hernández A., Thermodynamic modelling of a hybrid solar gas-turbine power plant. Ener. Conv. Manage. 2015;93:435-447.

[10] Collado F., Guallar J., A review of optimized design layouts for solar power tower plants with campo code. Renew. Sust. Energ. Rev. 2013;20;142-154.

[11] Zhang M., Yang L., Xu C., Du X., An efficient code to optimize the heliostat field and comparisons between the biomimetic spiral and staggered layout. Renew. Ener. 2016;87:720-730.

[12] Collado F. J., Preliminary design of surrounding heliostat fields. Renew. Ener. 2009;34:1359-1363.

[13] Gómez Cristóbal A. Proyecto Fin de Carrera – Diseño del campo de heliostatos para torres solares de receptor central. Universidad Carlos III de Madrid. 2011.

[14] Korzynietz R., Brioso J. A., del Río A., Quero M., Gallas M., Uhlig R.,Ebert M., Buck R., Teraji D., *Solugas* – Comprehensive analysis of the solar hybrid Brayton plant. Sol. Ener. 2016;135:578-589.

[15] Quero M., Korzynietz R., Ebert M., Jiménez A., del Río A., Brioso J. A., *Solugas* – Operation experience of the first solar hybrid gas turbine system at MW scale. Ener. Proc. 2014;49:1820-1830.

[16] Thermoflex. Available at: <https://www.thermoflow.com> [accessed 18.1.2019].

[17] Meteosevilla. http://www.meteosevilla.com. Available at: <http://www.meteosevilla.com> [accessed 18.1.2019].

[18] Caterpillar. Available at: <https://www.solarturbines.com> [accessed 18.1.2019].

[19] Stine W. B., Geyer M., Power from the Sun (2001). Available at: <http://www.powerfromthesun.net/book.html> [accessed 18.1.2019].